Journal of the Meteorological Society of Japan, Vol. 87A, pp. 153–164, 2009
DOI:10.2151/jmsj.87A.153

Development of Nonuniform Beamfilling Correction Method in Rainfall Retrievals for Passive Microwave Radiometers over Ocean Using TRMM Observations

Takuji KUBOTA

Earth Observation Research Center, Japan Aerospace and Exploration Agency, Tsukuba, Japan

Shoichi SHIGE

Department of Aerospace Engineering, Osaka Prefecture University, Sakai, Japan

Kazumasa AONASHI

Meteorological Research Institute, Japan Meteorological Agency, Tsukuba, Japan

and

Ken'ichi OKAMOTO

Faculty of Environmental and Information Studies, Tottori University of Environmental Studies, Tottori, Japan

(Manuscript received 17 June 2008, in final form 28 October 2008)

Abstract

Nonuniform beamfilling (NUBF) is a major error source in physical retrieval algorithms for estimating rain rates using satellite-borne passive microwave radiometers. The NUBF effects over the ocean within the beam effective field of view in the 10 GHz channel (FOV10) for the Tropical Rainfall Measuring Mission (TRMM) Microwave Imager (TMI) are investigated from simultaneous measurements made by the TMI and the Precipitation Radar (PR) aboard the TRMM satellite. They are investigated with respect to variability of a non-uniform parameter defined by the lognormal assumption from January to December 2000.

The parameter computed using surface rain rates estimated from PR data tends to be small (large) for stratiform (convective) rainfall in the FOV10. The parameter computed using surface rain rates estimated from brightness temperature (Tb) at 85 GHz is systematically lower in stratiform rainfall than the reference derived by the PR. Systematic differences are not found for the convective cases. To evaluate the effects on rain retrievals due to the systematic differences of the non-uniform parameters, a simple adjustment is applied, and rain retrievals from the observed TMI Tb at 10 GHz vertical polarization are performed over the ocean. Relatively large increases in rain rates retrieved using corrected parameters are found in the tropics, while the increases of the corrected parameters are similar for all latitudes. Effects of the non-uniform parameter differences on the rain retrievals are nonlinear and could be closely related to high background values of the non-uniform parameter in the tropics and more frequent high rainfall intensities.

Corresponding author: Takuji Kubota, Earth Observation Research Center, Japan Aerospace Exploration Agency, 2-1-1 Sengen, Tsukuba, Ibaraki 305-8505, Japan
E-mail: kubota@ieee.org

1. Introduction

Nonuniform beamfilling (NUBF) is a major error source in physical retrieval algorithms for estimating rain rates using satellite-borne passive microwave radiometers, as described in previous papers (e.g.,

Wilheit 1986; Chiu et al. 1990; Short and North 1990). It is necessary to consider nonuniform rainfall within the field of view (FOV) of the radiometers to quantify the effects of the NUBF. Turk et al. (1998) examined the effects of degraded sensor resolution in passive microwave radiometers aboard satellites upon retrievals of tropical rainfall using fine-scale data derived from aircraft-based instruments. Kummerow et al. (2004) discussed the effects of NUBF errors on the climate variability of rainfall estimated using passive microwave sensors.

Kummerow and Giglio (1994, hereafter, KG94) proposed a procedure in which relationships between rain rates and brightness temperatures (Tbs) derived from a plane-parallel radiative transfer model (RTM) are corrected by lognormal distributions estimated from high-resolution 85 GHz Tbs data (Tb_{85}s). They noted differences between estimations of lognormal distributions from Tb_{85}s and radars over the Tropical Ocean Global Atmosphere Coupled Ocean Atmosphere Response Experiment (TOGA COARE) domain located in the western Pacific. Kummerow (1998) examined the impact of inhomogeneous rainfall upon the predicted Tbs using either lognormal or gamma distributions to develop a physically based error model for microwave precipitation retrievals.

According to KG94, the NUBF correction method using the lognormal distribution is as follows. Rainfall is assumed to be distributed lognormally as observed in Biondini (1976), Houze and Cheng (1977), Kedem et al. (1990), and other works. It is then possible that the RTM-derived Tb–rain relations are modified as a function of the variability ζ,

$$Tb_{correct}\left(\langle R\rangle,\zeta\right)=\int_0^{\infty} Tb(R)\frac{1}{(2\pi)^{1/2}\zeta R}\exp\left\{\frac{-1}{2\zeta^2}\left[\ln(R)-\mu\right]^2\right\}dR. \quad (1)$$

Here, $\zeta^2=\ln\left(\sigma^2+1\right)^2$, $\mu=\ln\left(\langle R\rangle\right)-0.5\zeta^2$, Tb(R) is the RTM-derived Tb–rain relation, $Tb_{correct}$ is the Tb–rain relation corrected by the lognormal distribution, R is the rain rate, and $\langle R\rangle$ is the mean rain rate of the lognormal distribution. For the FOV of the low frequency channels, σ is defined using rain rates estimated from Tb_{85}s as

$$\sigma=\frac{\left[\frac{1}{N}\sum_{i=1}^{N}\left(R_i-R_{avg}\right)^2\right]^{1/2}}{R_{avg}}. \quad (2)$$

Here, i represents each pixel of the 85 GHz data within the FOV area of the low frequency data, and N is the total number of pixels in the area. In Eq. (2), R_i is the rain rate of the 85 GHz data pixels and R_{avg} is the average in the FOV area of the low frequency data. Rain rates are retrieved from low frequency Tb data using the relationship between rainfall and $Tb_{correct}$ for ζ derived from 85 GHz Tb data. Figure 1 presents an example of a rain–Tb relation for Tbs at 10-GHz vertical polarization (Tb_{10vs}) over the mid-latitude ocean (147.5°E, 32.5°E) on January 1, 2000. Here, ζ is

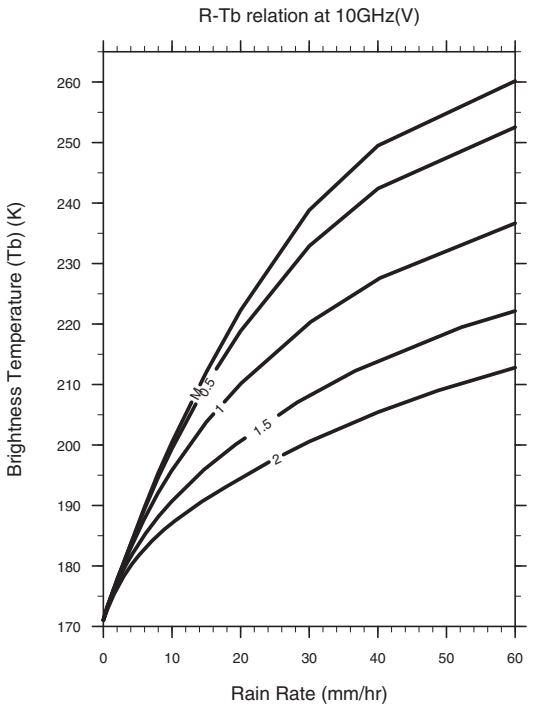

Fig. 1. Example of a rain–Tb relation for Tbs at 10-GHz vertical polarization over the mid-latitude ocean (147.5°E, 32.5°N) on January 1, 2000. The horizontal (vertical) axis denotes the rain rate (calculated Tb). The line labeled "M" denotes values calculated using a plane-parallel RTM; lines labeled "0.5", "1", "1.5", and "2" denote values calculated with rainfall inhomogeneity ζ in the lognormal distribution of 0.5, 1, 1.5, and 2, respectively.

regarded as a non-uniform parameter. Similar relations are found in Fig. 3 of Kummerow (1998) and Fig. 2 of Kubota et al. (2007). In Fig. 1, the line for Tb(R) is labeled as "M", while lines labeled "0.5", "1", "1.5", and "2" denote values of $Tb_{correct}(\langle R\rangle, \zeta)$ with ζ of 0.5, 1, 1.5, and 2, respectively. Figure 1 clearly depicts the effects of NUBF, in that for the same Tb intensity stronger rain rates are retrieved for larger values of the rainfall inhomogeneity ζ and the relationship between Tb, rain rate, and a given ζ is not linear.

Simultaneous rain observations have been performed aboard the Tropical Rainfall Measuring Mission (TRMM) satellite by the TRMM Microwave Imager (TMI) and Precipitation Radar (PR) (Kummerow et al. 1998, 2000). By analyzing collocated TMI and PR data, Varma et al. (2004) demonstrated that a simulation by a plane-parallel RTM significantly underestimates in convective rainfall events with reference to the averaged relationship beween observed Tbs and rain rates at 19 and 37 GHz. Varma and Liu (2006) suggested the parameterization of fractional rain cover (FRC) and conditional rain-rate probability density functions (PDFs), based upon three years of PR data. Their approach is an application of statistical parameterization to observed Tbs, while the approach of the KG94 method is an estimation of the NUBF effect from instantaneous satellite observations.

In this study, the method of the lognormal distribution based upon the KG94 procedure is investigated over the ocean within the beam effective FOV in the 10 GHz channel (FOV10) for the TMI (63 km × 37 km) using simultaneous measurements made by the TMI and PR. The simultaneous measurements by the two sensors enable us to examine the NUBF effects in the overall region observed by the TRMM. The over-ocean algorithm for the microwave radiometers uses emission signals from low frequency channels such as the 10 GHz channel in addition to scattering signals from high frequency channels such as the 85 GHz channel, while the over-land algorithm uses just scattering signals because of the high and variable emissivity of the land surface. Thus, we focus on analyses of the NUBF effects over the ocean.

Values of instantaneous ζ estimated from TMI Tb_{85} and PR data are compared, and then possible systematic differences are found between them. Datasets are briefly described in Section 2. The features of ζ are documented in Section 3. Section 3 also compares results using TMI Tb_{85} and PR data. We try simple corrections for systematic differences and apply them to the TMI retrievals. A summary is presented in Section 4.

2. Data used in this study

The NUBF effects are investigated with respect to ζ from January to December 2000 in this study. Analyzed cases are restricted to those with fractional rain cover (FRC) above 50% in the FOV10, because moderate numbers of pixels for which there is rain are necessary to establish the lognormal assumption. To quantitatively estimate the instantaneous NUBF effect, ζ values are computed from two different datasets, rain rate estimated from TMI Tb_{85} (rainTMI85) and rain rate estimated from PR data (rainPR).

2.1 rainTMI85

The rain rate, rainTMI85, is retrieved from the observed polarization-corrected temperature (PCT, Spencer et al. 1989) recorded at 85.5 GHz by the TMI using an RTM calculation, with statistically classified vertical profiles of precipitation observed by the PR, and background meteorological variables taken from the Japan Meteorological Agency Global Analysis dataset. This retrieval method is based upon an algorithm developed by the Global Satellite Mapping of Precipitation (GSMaP) Project (Okamoto et al. 2005, 2007); a detailed description is provided by Aonashi and Liu (2000), Kubota et al. (2007) and Aonashi et al. (2009). Rain identification over the ocean for rainTMI85 is based on either "rainTMI85 > 1 mm h^{-1}" or "observed Tb at 37 GHz (v) (Tb_{37v}) > Tb_{37v} calculated by the RTM for the no-rain condition", according to the results of Kida et al. (2009). A four-stream RTM developed by Liu (1998) is used here. The beam effective FOV for the 85 GHz channel is 7 km × 5 km. In this study, the analyses are performed for cases with two or more pixels having rainTMI85 above 0 mm h^{-1} in the FOV10. Hereafter, ζ omputed using rainTMI85 is referred to as "ζ_{m85}".

2.2 rainPR

The TRMM PR is the first spaceborne Precipitation Radar, and its 128-element active phased-array system operates at 13.8 GHz (Okamoto 2003; Kozu et al. 2001; Iguchi et al. 2000; Okamoto and Shige 2008). We use estimated surface rain by PR 2A25 Version 6 as rainPR. The horizontal resolution is 4.3 km at nadir. In this study, the analyses are performed for cases with two or more pixels having rainPR above 0 mm h^{-1} in the FOV10. Hereafter, ζ computed using rainPR is referred to as "ζ_{rpr}".

2.3 Convective/stratiform rain area and rain ratio

In this paper, a stratiform rain ratio (SRR) over the FOV10 (63 km × 37 km window) is used for analyses. The SRR is a ratio of the total rain amount to the stratiform rain amount defined in the following equation.

$$SRR = \frac{\sum_{i=1}^{N} (f_{strat} \cdot R_i)}{\sum_{i=1}^{N} R_i} . \quad (3)$$

Here, i represents each pixel within the FOV10 area, N is the total number of pixels in the area, and R_i is the rain rate. f_{strat} is derived from rain-type classification algorithms, which differ between the PR and the TMI. The TRMM PR rain-type classification algorithm uses two independent methods (Awaka et al. 2007). One is a vertical profile method (Awaka et al. 1998), and the other is a horizontal pattern method (Steiner et al. 1995). Combined results of the two methods classify rain for a PR pixel as stratiform, convective, or other. Using PR data, f_{strat} is a discrete value, and is 0 for convective rainfall and 1 for stratiform rainfall. For the TMI algorithm, the method for the TMI Goddard Profiling Algorithm (GPROF) Version 6 described in Olson et al. (2001, 2006) is used here. The area fraction of convective rainfall within the TMI footprint is computed, combining convective fraction estimates from both TMI polarization signatures and image texture. Using TMI data, f_{strat} is a continuous value between 0 and 1.

3. Non-uniform parameter ζ and its influence on rain retrievals

3.1 Features of ζ determined from PR data

In this section, features of ζ_{rpr} are noted for comparison between ζ_{rpr} and ζ_{m85}. Figure 2 plots horizontal distributions of ζ_{rpr} averaged from January to March or July to September 2000. Cases with FRC above 50% in the FOV10 are analyzed here. In both periods, ζ_{rpr} values are smaller than 0.9 over the winter mid-latitude ocean, while they exceed 1.1 over the subtropical ocean. Stratiform rainfall dominates at mid latitude (Schumacher and Houze 2003). Thus, variances are relatively small, and ζ_{rpr} values, which are related to variances divided by averages, are small. However, isolated convections dominate in the subtropics (Short and Nakamura 2000; Schumacher and Houze 2003) and ζ_{rpr} values are large. In contrast, the

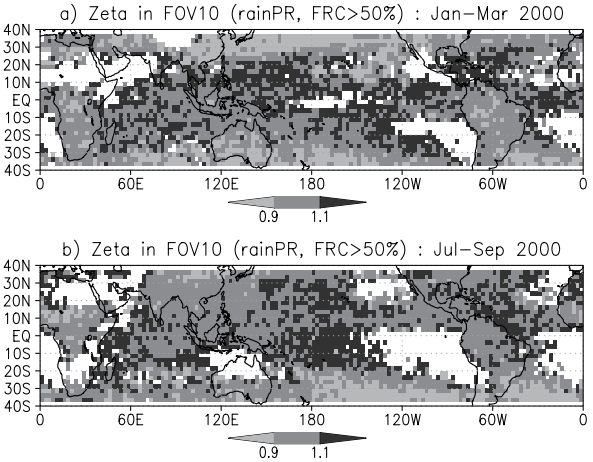

Fig. 2. Seasonally averaged values of non-uniform parameter ζ in the TMI 10 GHz FOV computed using PR surface rain. Values of ζ are averaged in 2.5 × 2.5° latitude/longitude boxes and a) from January to March 2000 or b) from July to September 2000. Cases are selected for FRCs above 50%. Darker colors represent larger values; white indicates missing values.

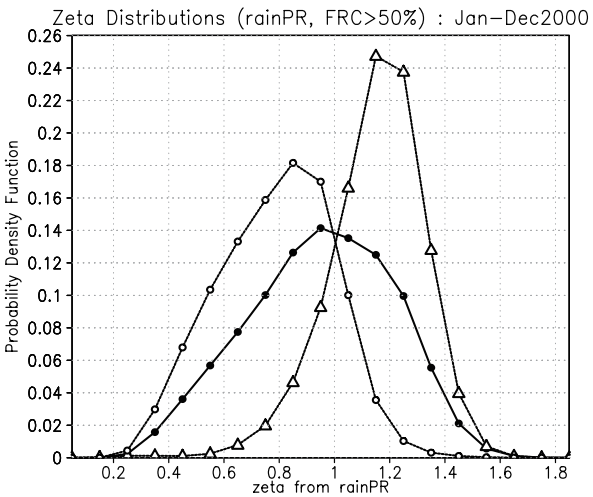

Fig. 3. Probability density function (PDF) of ζ_{rpr} for all cases (solid circles), convective cases (open triangles), and stratiform cases (open circles) from January to December 2000. The bin width of the horizontal axis is 0.1.

values of ζ_{rpr} are moderate over the South Pacific convergence zone (SPCZ) during the boreal winter and the intertropical convergence zone (ITCZ) during the boreal summer, although the rainfall amounts are large in those areas. This is because precipitation systems, which are organized by convective and stratiform regions, contribute to the large rainfall amount. Houze (1977) indicated that stratiform rainfall accounted for 40% of the total for a tropical squall line system observed during the Global Atmospheric Research Program (GARP) Atlantic Tropical Experiment (GATE). Using the TRMM PR data, Schumacher and Houze (2003) demonstrated that the ITCZ has more moderate stratiform rain fractions and is more clearly delineated from regions outside of the ITCZ. Thus, organized systems as seen in the ITCZ are quite different from isolated convections as seen in the subtropics.

The ζ_{rpr} distributions are analyzed in terms of the rain-type classification. Figure 3 presents the probability density functions (PDFs) of ζ_{rpr} in all cases, convective cases, and stratiform cases from January to December 2000. Here, convective (stratiform) cases have SRRs below 10% (above 90%) over the FOV10 based on PR data. There was a total of 4918045, of which 46622 were convective and 2444648 were stratiform. In this definition, the number of the convective cases is much smaller than the number of the stratiform cases, because an organized convective system is not included in the "convective" cases, and a relatively large amount of rainfall is observed in the stratiform region of the system. Considering all cases, a peak is found around 0.95, while a peak is found around 0.85 (1.15) for stratiform (convective) cases. In the stratiform cases, 85% of ζ_{rpr} values are below 1.0, while 83% of ζ_{rpr} values are above 1.0 in the convective cases. Thus, ζ_{rpr} tends to be small (large) for stratiform (convective) rain defined by the rainPR in the FOV10.

3.2 *Comparison of ζ values determined using TMI and PR data*

This section compares ζ_{m85} with the reference ζ_{rpr} from January to December 2000. Analyzed cases are restricted to FRC above 50% using rainPR in the previous section. In this section, the cases are restricted using both rainPR and rainTMI85 to elim-

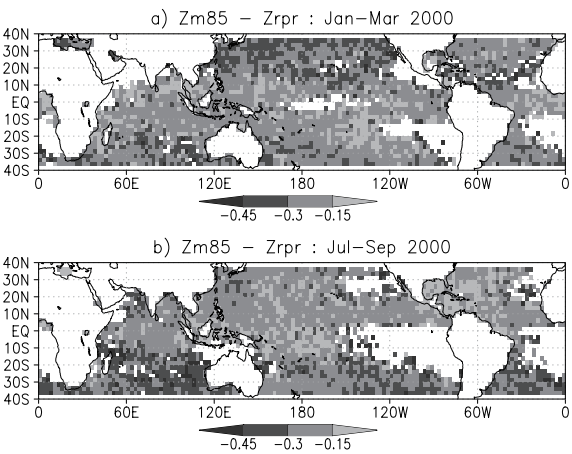

Fig. 4. Seasonally averaged differences between ζ_{m85} and ζ_{rpr}. Values are averaged in 2.5 × 2.5° latitude/longitude boxes and a) from January to March 2000 or b) from July to September 2000. Darker colors represent smaller values; white indicates missing values.

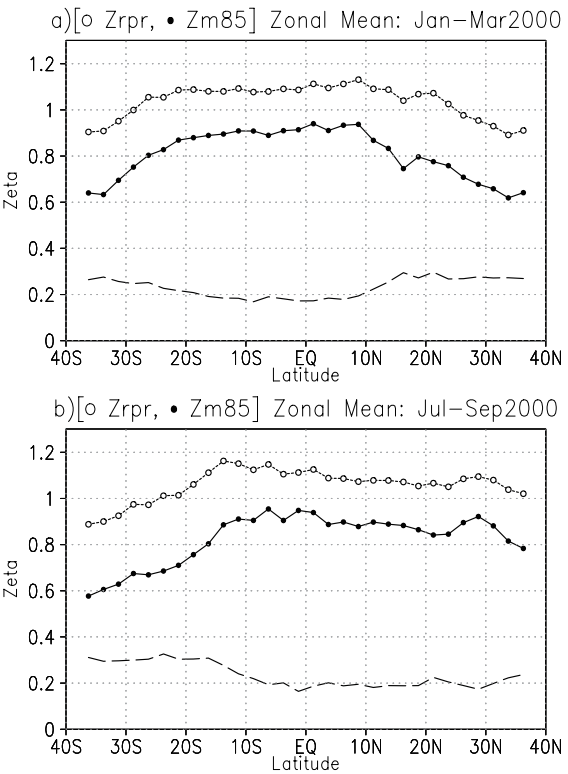

Fig. 5. Zonally averaged ζ_{m85}, ζ_{rpr}, and differences between ζ_{m85} and ζ_{rpr}. Values are averaged a) from January to March 2000 or b) from July to September 2000. Solid (open) circles denote ζ_{m85} (ζ_{rpr}). A dashed line indicates differences (i.e., ζ_{m85} minus ζ_{m85}).

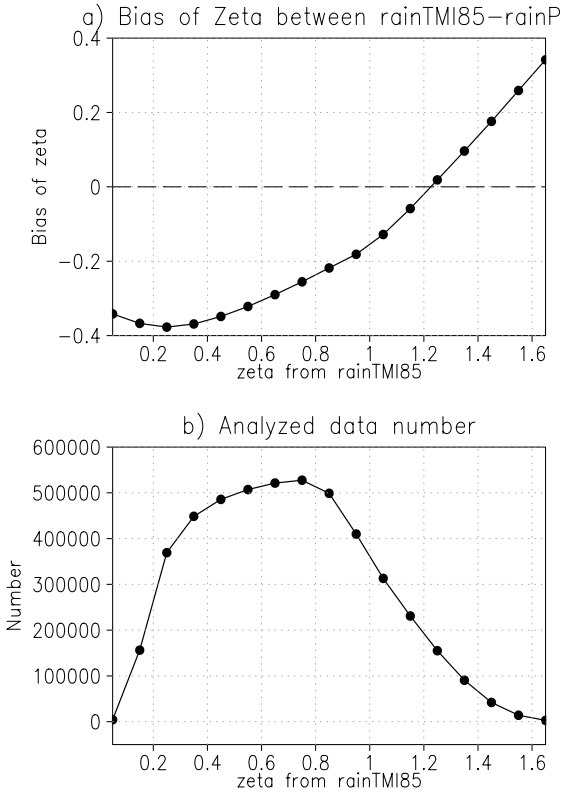

Fig. 6. a) Differences between ζ_{m85} and ζ_{rpr} with respect to intensity of ζ_{m85} from January to December 2000. Analyzed data numbers are displayed in b).

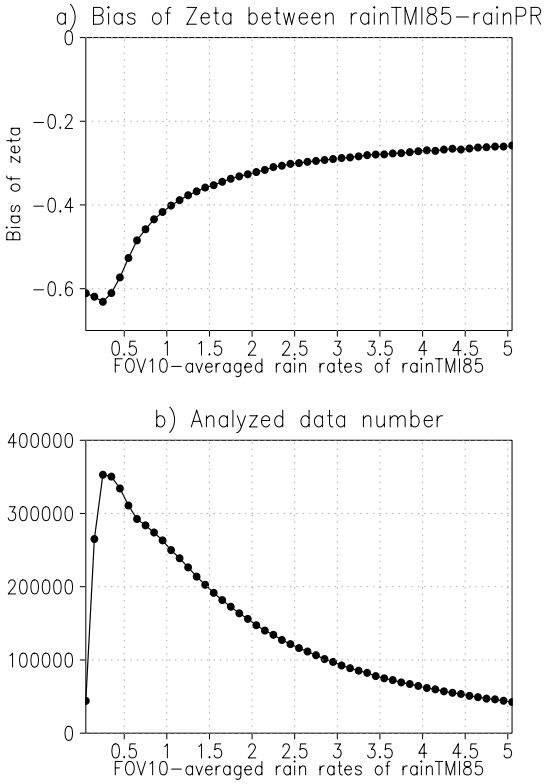

Fig. 7. Same as Fig. 6, but with respect to FOV10-averaged rainTMI85.

inate rain identification problems.

Figure 4 plots seasonally averaged differences defined as "ζ_{m85} minus ζ_{rpr}". Values of ζ_{m85} are 0.3 lower than those of ζ_{rpr} over the winter mid-latitude ocean, while differences are relatively small over the subtropical ocean. As illustrated in Fig. 2, ζ_{rpr} is smaller in the winter mid-latitude ocean than in other regions and the differences between ζ_{rpr} and ζ_{m85} are larger in this region. Figure 5 depicts zonally averaged ζ_{m85}, ζ_{rpr}, and differences between ζ_{m85} and ζ_{rpr}. Values of ζ tend to be about 0.2 smaller in the mid-latitudes, in particular, in the winter hemisphere, than in the tropics. In contrast the differences between ζ_{m85} and ζ_{rpr} are 0.1 larger in mid-latitudes.

Differences of ζ_{m85} and ζ_{rpr} are quantitatively analyzed in Figs. 6 and 7 with respect to the intensity of ζ_{m85} and averaged rainTMI85. In Fig. 6a, ζ_{m85} is lower than ζ_{rpr} when ζ_{m85} is smaller than 1.2, and is higher when ζ_{rpr} is larger than 1.2. However, there are many more cases of ζ_{m85} below 1.2 than there are above 1.2 (Fig. 6b). Values of ζ_{m85} are about 0.4 lower than those of ζ_{rpr} when ζ_{m85} is 0.2 to 0.3. Figure 7a illustrates the relationship between the differences and rainTMI85 averaged in the FOV10, showing that ζ_{m85} is systematically lower than ζ_{rpr} when the averaged rainTMI85 is less than 1 mm h^{-1} . This suggests that the poor sensitivity of rainTMI85 to weak rain rates causes large differences because Tbs at 85 GHz is sensitive to scattering of ice particles.

Furthermore, the differences between ζ_{m85} and ζ_{rpr} are analyzed in terms of the rain-type classification. Figure 8 presents the differences with respect to the intensity of the SRR, which is derived from the PR or the TMI. For both SRR values, differences of ζ are larger for high SRR values than for low values. Figure 8b shows that there are many more cases of high SRR values than low values. Figure 9 plots two-dimensional PDFs in terms of ζ_{m85} and ζ_{rpr} for stratiform cases from January to December 2000. The definition of a stratiform case is the same as that used in Fig. 3. Figure 9 indicates that ζ_{rpr} is about 0.3 higher than

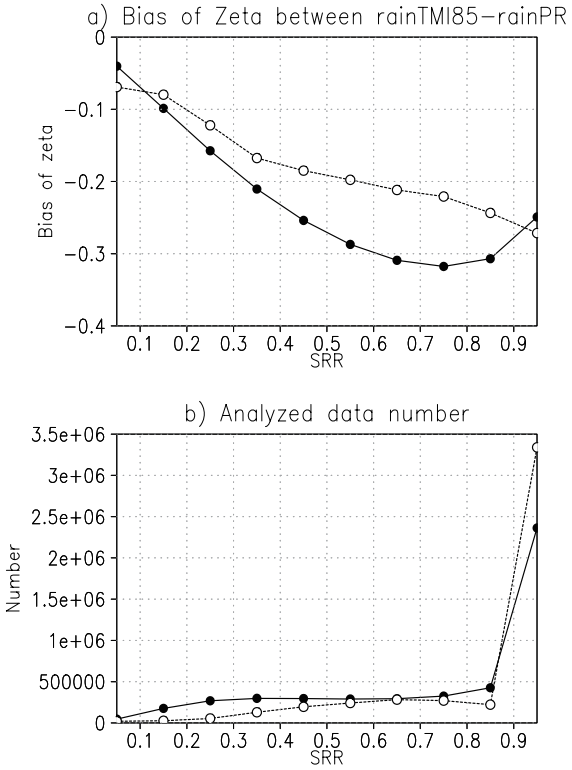

Fig. 8. Differences between ζ_{m85} and ζ_{rpr} from January to December 2000 analyzed with respect to intensity of SRR. Solid circles denote results of SRR from the PR, and open circles denote results of SRR from the TMI. Analyzed data numbers are displayed in b).

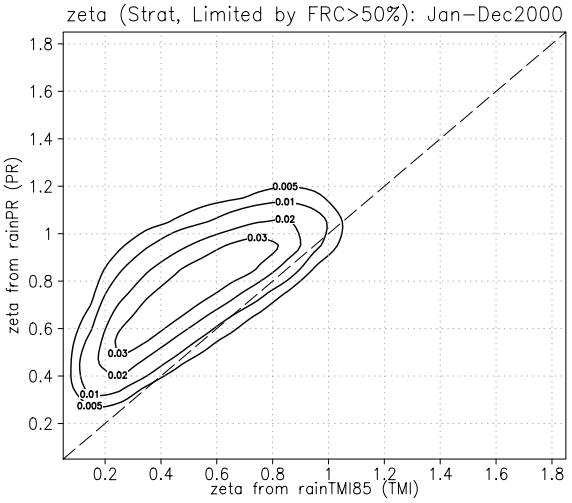

Fig. 9. Two-dimensional PDFs in terms of ζ_{m85} (horizontal axis) and ζ_{rpr} (vertical axis) for stratiform cases from January to December 2000. Contours show labeled values. Cases are selected for FRCs above 50%.

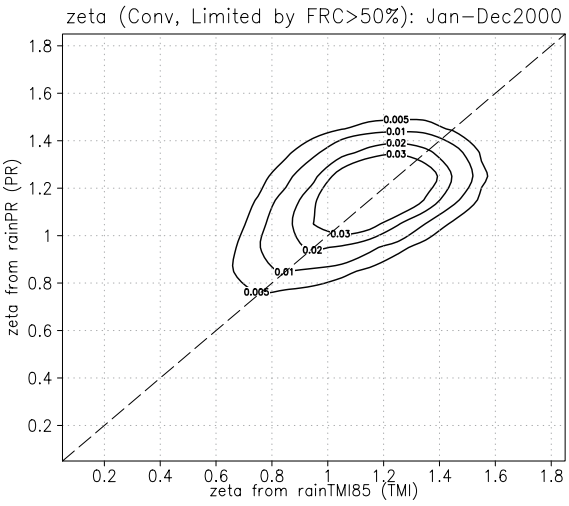

Fig. 10. Same as Fig. 9, except for convective cases.

ζ_{m85} in stratiform cases and that the variations in ζ_{m85} correspond well to those in ζ_{rpr}. The correlation coefficient between ζ_{m85} and ζ_{rpr} is 0.70, and 2362625 stratiform cases were analyzed. Figure 10 presents the results for convective cases; no systematic differences are found for the convective cases. The correlation coefficient between ζ_{m85} and ζ_{rpr} is 0.53, and 45733 convective cases were analyzed.

3.3 Actual effects on rain retrievals using differential ζ values

Differences of ζ values determined using TMI and PR data are large in stratiform rainfall. To evaluate the effects of the systematic differences on rain retrievals, we adopt the following simple correction for ζ_{m85},

$$\zeta^{*}_{m85} = \zeta_{m85} + C_{\mathrm{diff}}(\mathrm{SRR}). \quad (4)$$

Here, an SRR value is computed from the TMI defined in Eq. (3). C_{diff} is the value of the averaged differences defined as "ζ_{rpr} minus ζ_{m85}" (in other words, the differences depicted by open circles of Fig. 8a multiplied by –1) and is a function of the intensity of SRR derived from the TMI. Thus, if we use the same analysis for ζ^{*}_{m85} as that used in Fig. 8a with the

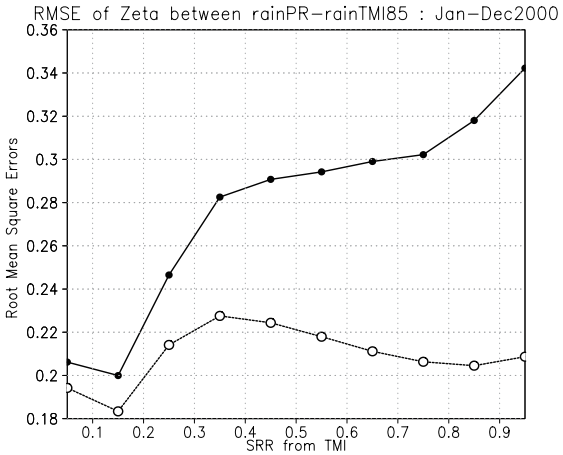

Fig. 11. RMSEs of ζ_{m85} and ζ_{rpr} from January to December 2000 with respect to intensity of SRR from the TMI. Solid circles represent uncorrected results; open circles, corrected results.

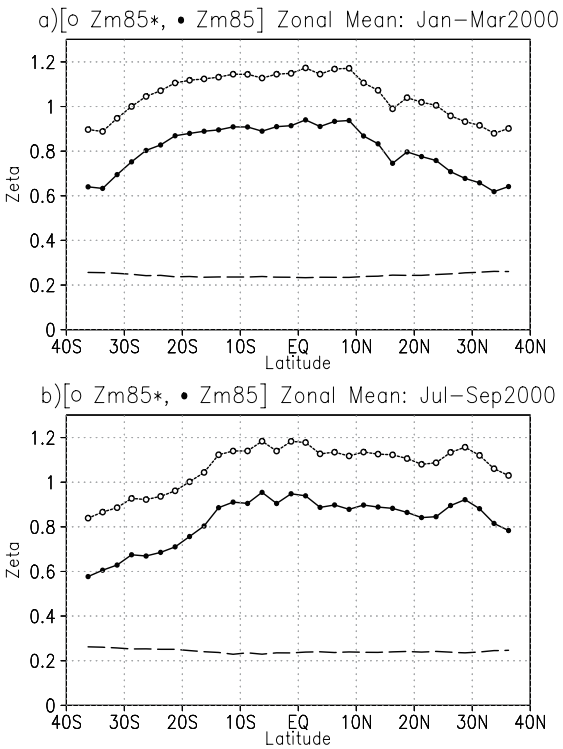

Fig. 12. Zonally averaged ζ_{m85}, ζ^*_{m85}, and differences between ζ_{m85} and ζ^*_{m85}. Values over the ocean are averaged a) from January to March 2000 or b) from July to September 2000. Solid (open) circles denote ζ_{m85} (ζ^*_{m85}). Dashed line indicates differences (i.e., ζ^*_{m85} minus ζ_{m85}).

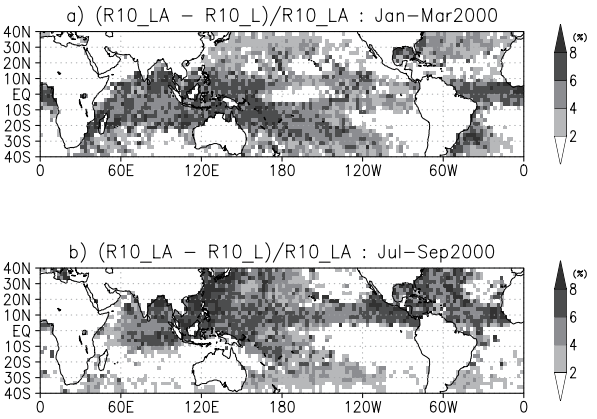

Fig. 13. Normalized differences "R_{diff}" between R10_LA and R10_L, averaged a) from January to March or b) from July to September 2000. The differences are percentages. The horizontal resolution is 2.5 × 2.5° latitude/longitude. Darker colors represent larger values.

SRR from the TMI, there will be no differences. On the other hand, small root mean square errors (RMSEs) are not guaranteed and the RMSEs for ζ_{m85} and ζ^*_{m85} are compared in Fig. 11. In Fig. 11, data are binned according to SRR values. Figure 11 shows that RMSEs are significantly less using ζ^*_{m85}. Average values of RMSE for ζ_{m85} and ζ^*_{m85} are 0.33 and 0.21, respectively, showing that RMSEs decrease by an average of 64% when using the ζ adjustment. Figure 12 depicts zonally averaged ζ_{m85}, ζ^*_{m85}, and differences between ζ_{m85} and ζ^*_{m85}. The differences are similar for all latitudes, while slight increases are found at mid-latitudes. Comparison with Fig. 12 and Fig. 5 for the ζ_{m85} reveals that ζ^*_{m85} derived by the current simple method is over-corrected less than 0.1 in zonal averages in the tropics.

To examine the effects of the above ζ adjustment, we retrieved rain rates using ζ_{m85} and ζ^*_{m85} from observed TMI Tb_{10v}s. The retrieval method is based upon the RTM calculation and is the same as that described in Section 2.1 for rainTMI85. In this experiment design, the NUBF correction method using the lognormal distribution is applied to FRC above 50% in the FOV10. Rain retrievals using ζ_{m85} (ζ^*_{m85}) are referred to as "R10_L" ("R10_LA"). Figure 13 depicts the difference, that is, "R10_LA minus R10_L", divided by R10_LA, which is defined as "R_{diff}". In the adjustment method, ζ^*_{m85} is larger than ζ_{m85} for all values of SRR. The Tb relations with rainfall for

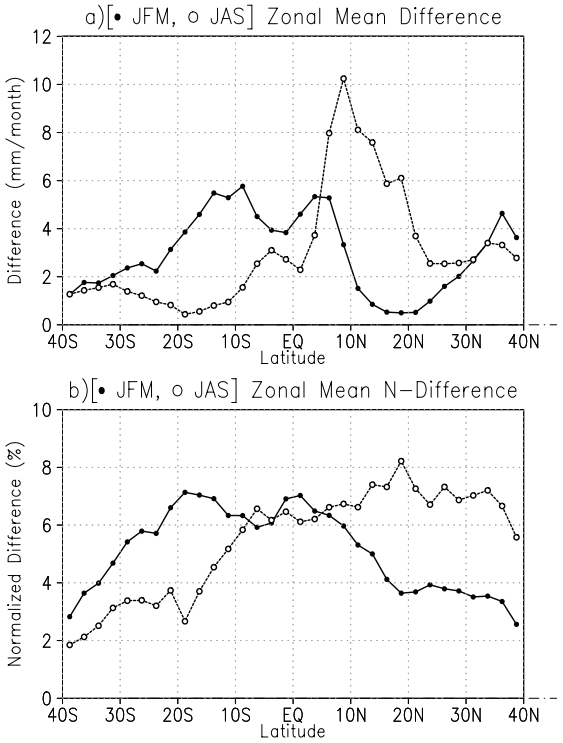

Fig. 14. Zonally averaged differences between surface rain rates of R10_LA and R10_L. Solid (open) circles denote values averaged from January to March 2000 (July to September 2000). Panel a shows differences (mm month^{-1}); Panel b, normalized differences (%).

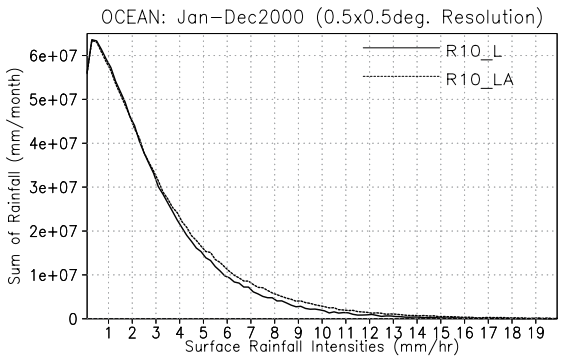

Fig. 15. Histogram showing the sum rainfall for different rain rates over the ocean from January to December 2000. Solid (dashed) lines indicate rain rates of R10_L (R10_LA). This analysis is for daily 0.5 × 0.5° boxes. The width of the histogram bin is 0.02 mm h^{-1}.

various ζ values of the lognormal distribution, as shown in Fig. 1, suggest increases in retrieved rain rates with increases in ζ. The rain rates increase when using ζ^*_{m85} instead of ζ_{m85} over global rainfall areas. R_{diff} averaged over the ocean from 40°S to 40°N from January to December 2000 is 5.5%.

In Fig. 13, more large differences are seen in the tropics than in the mid-latitudes. Figure 14 presents zonally averaged differences between surface rain rates of R10_LA and R10_L. Figure 14 compares differences, in addition to normalized differences. Figure 14 also demonstrates that differences between R10_LA and R10_L are relatively large in the tropics. In contrast, increases of ζ are similar for all latitudes (Fig. 12). There are two possible reasons. First is the background intensity of ζ. As indicated in Figs. 5 and 12, values of ζ are larger in the tropics than in the mid-latitudes. The relationship between Tb and rain rate is more sensitive to the intensity of ζ when the intensity of ζ is larger. For example, Fig. 1 shows differences between rain rates retrieved for ζ = 1 and ζ = 1.5 from the same Tbs are larger than those retrieved for ζ = 0.5 and ζ = 1. Thus, more increases of rain rates derived from the ζ adjustment in the tropics can be related to the high background values of ζ there.

The second reason is that there are more frequent high rain rates in the tropics. Figure 1 also suggests increases in retrieved rain rates are larger when intensities of rain are stronger for the same positive increment of ζ. For example, rain rates of ζ = 0.5 and ζ = 1 for Tb=200 (K) are 10.3 and 12.6 mm h^{-1} and those for Tb=210 (K) are 15.0 and 20.0 mm h^{-1}, respectively (Fig. 1). This implies that there are large increases in rain rates retrieved in the tropics where strong rainfall intensities and high Tb_{10v}s due to them are more frequently observed. Figure 15 is a histogram showing the sum rainfall for different rain rates over the ocean from January to December 2000, indicating the contribution of specific rain intensities to the total rainfall amount. This analysis is done for daily 0.5 × 0.5° boxes. Figure 15 demonstrates clear increases (slight decreases) in the summation of rainfall above (below) 2.0 mm h^{-1} using ζ^*_{m85}. Thus, the ζ adjustment of ζ_{m85} can result in more frequent high rainfall intensities.

4. Summary

The NUBF effects over the ocean within the FOV10 for TMI were investigated from simultaneous measurements made by TMI and PR aboard the TRMM

satellite. They are examined in overall regions observed by the TRMM with respect to ζ of the lognormal distribution for cases with FRC above 50% in the FOV10 from January to December 2000. ζ_{rpr}, which is ζ determined from rainPR, is less than 0.9 over the mid-latitude ocean and exceeds 1.1 over the subtropical ocean. ζ_{rpr} tends to be small (large) for stratiform (convective) rain in the FOV10. Here, convective (stratiform) rain cases have SRRs, which are ratios of the total rain amount to the stratiform rain amount using 2A25 rain-type classification, below 10% (above 90%) over the FOV10.

ζ_{m85}, which is ζ determined from rainTMI85, is compared with ζ_{rpr} from January to December 2000. ζ_{m85} is systematically lower than ζ_{rpr} over the winter mid-latitude ocean, while differences are relatively small over the subtropical ocean. ζ_{m85} is systematically lower than ζ_{rpr} for stratiform rainfall, with the variations in ζ_{m85} corresponding well to those of ζ_{rpr}. Large differences are found when rain rates of the rainTMI85 averaged over the FOV10 are less than 1 mm h^{-1}. No systematic difference is found for the convective cases. To evaluate the effects of the systematic differences of ζ on rain retrievals, a simple adjustment is applied to ζ_{m85}. The adjustment of ζ leads to an average 5.5% increase in rain retrievals from the observed TMI Tb_{10v} over the ocean. The effects of the non-uniform parameter differences on the rain retrievals are nonlinear, and relatively large increases in retrieved rain rates are found in the tropics, while the increases of ζ are similar for all latitudes. It is suggested that this can be closely related to high background values of ζ in the tropics and more frequent high rainfall intensities.

In this paper, the NUBF effects are analyzed for cases of FRC above 50%. This threshold is used because a certain number of rain pixels is necessary to establish the lognormal assumption. For small rain area cases, parameterization based upon PR data can be effective, as demonstrated by Varma and Liu (2006).

Acknowledgements

This study was partly supported by "Production of a High-Precision, High-Resolution Global Precipitation Map Using Satellite Data" (the GSMaP project) under the "Core Research for Evolutional Science and Technology" (CREST) program of the Japan Science and Technology Agency (JST), and partly by the Fifth TRMM Japanese Research Announcement of the Japan Aerospace Exploration Agency (JAXA). The authors would like to thank the members of the GSMaP Project for many valuable comments. They use a part of 2A12 source programs for detection of convective/nonconvective rain area. We thank Prof. C. D. Kummerow (Colorado State University) for providing 2A12 programs and valuable suggestions. They would also like to thank Dr. G. Liu (Florida State University) for the RTM code. Figures were drawn using the Grid Analysis and Display System and GFD-DENNOU Library.

References

Aonashi, K., and G. Liu, 2000: Passive microwave precipitation retrievals using TMI during the Baiu period of 1998 Part I: Algorithm description and validation. *J. Appl. Meteor.*, **39**, 2024–2037.

Aonashi, K., J. Awaka, M. Hirose, T. Kozu, T. Kubota, G. Liu, S. Shige, S. Kida, S. Seto, N. Takahashi, and Y. N. Takayabu, 2009: GSMaP passive microwave precipitation retrieval algorithm: Algorithm description and validation, *J. Meteor. Soc. Japan*, **87A**, 119–136.

Awaka, J., T. Iguchi, and K. Okamoto, 1998: Early results on rain type classification by the Tropical Rainfall Measuring Mission (TRMM) Precipitation Radar. *Proc. URSI-F Open Symp. on Wave Propagation and Remote Sensing*, Aveiro, Portugal, 143–146.

Awaka, J., T. Iguchi, and K. Okamoto, 2007: Rain type classification algorithm. *Measuring precipitation from space EURAINSAT and the future*, Springer, 213–224.

Biondini, R., 1976: Cloud motion and rainfall statistics. *J. Appl. Meteor.*, **15**, 205–224.

Chiu, L., G. North, D. Short, and A. McConnell, 1990: Rain estimation from satellites: Effect of finite field of view, *J. Geophys. Res.*, **95**, 2177–2185.

Houze, R. A., Jr., 1977: Structure and dynamics of a tropical squall-line system. *Mon. Wea. Rev.*, **105**, 1540–1567.

Houze, R. A., Jr., and C.-P. Cheng, 1977: Radar characteristics of tropical convection observed during GATE: Mean properties and trends over the summer season. *Mon. Wea. Rev.*, **105**, 964–980.

Iguchi, T., T. Kozu, R. Meneghini, J. Awaka, and K. Okamoto, 2000. Rainprofiling algorithm for the TRMM Precipitation Radar. *J. Appl. Meteor.*, **39**, 12, 2038–2052.

Kedem, B., L. Chiu, and G. North, 1990: Estimation

of mean rain rate: Application to satellite observations, *J. Geophys. Res*., **95**(D2), 1965–1972.

Kida, S., S. Shige, T. Kubota, K. Aonashi, and K. Okamoto, 2009: Improvement of rain/no-rain classification methods for microwave radiometer observations over the ocean using a 37 GHz emission signature, *J. Meteor. Soc. Japan*, **87A**, 165–181.

Kozu, T., T. Kawanishi, H. Kuroiwa, M. Kojima, K. Oikawa, H. Kumagai, K. Okamoto, M. Okumura, H. Nakatsuka, and K. Nishikawa, 2001: Development of precipitation radar onboard the Tropical Rainfall Measuring Mission satellite. *IEEE Trans. Geosci. Remote Sens*., **39**, 1, 102–116.

Kubota, T., S. Shige, H. Hashizume, K. Aonashi, N. Takahashi, S. Seto, M. Hirose, Y. N. Takayabu, K. Nakagawa, K. Iwanami, T. Ushio, M. Kachi, and K. Okamoto, 2007: Global precipitation map using satelliteborne microwave radiometers by the GSMaP project : Production and validation, *IEEE Trans. Geosci. Remote Sens*., **45**, 7, 2259–2275.

Kummerow, C., 1998: Beamfilling errors in passive microwave rainfall retrievals. *J. Appl. Meteor.*, **37**, 356–370.

Kummerow, C., and L. Giglio, 1994: A passive microwave technique for estimating rainfall and vertical structure information from space. Part I: Algorithm description, *J. Appl. Meteor.*, **33**, 3–18.

Kummerow, C., W. Barnes, T. Kozu, J. Shiue, and J. Simpson, 1998: The Tropical Rainfall Measuring Mission (TRMM) sensor package, *J. Atmos. Oceanic Technol*., **15**, 808–816.

Kummerow, C., J. Simpson, O. Thiele, W. Barnes, A. T. C. Chang, E. Stocker, R. F. Adler, A. Hou, R. Kakar, F. Wentz, P. Ashcroft, T. Kozu, Y. Hong, K. Okamoto, T. Iguchi, H. Kuroiwa, E. Im, Z. Haddad, G. Huffman, B. Ferrier, W. S. Olson, E. Zipser, E. A. Smith, T. T. Wilheit, G. North, T. Krishnamurti, and K. Nakamura, 2000: The status of the Tropical Rainfall Measuring Mission (TRMM) after two years in orbit. *J. Appl. Meteor.*, **39**, 1965–1982.

Kummerow, C., P. Poyner, W. Berg, and J. Thomas-Stahle, 2004: The effects of rainfall inhomogeneity on climate variability of rainfall estimated from passive microwave sensors. *J. Atmos. Oceanic Technol*., **21**, 624–638.

Liu, G., 1998: A fast and accurate model for microwave radiance calculations. *J. Meteor. Soc. Japan*, **76**, 335–343.

Okamoto, K., 2003: *A short history of the TRMM Precipitation Radar. Cloud Systems, Hurricanes and the Tropical Rainfall Measurement Mission (TRMM): A Tribute to Dr. Joanne Simpson, Meteor. Monogr.*, **29**, 51, Amer. Meteor. Soc., 187–195.

Okamoto, K., T. Iguchi, N. Takahashi, K. Iwanami, and T. Ushio, 2005: The global satellite mapping of precipitation (GSMaP) project, *25th IGARSS Proceedings*, 3414–3416.

Okamoto, K., T. Iguchi, N. Takahashi, T. Ushio, J. Awaka, S. Shige, and T. Kubota, 2007: High precision and high resolution global precipitation map from satellite data, *ISAP 2007 Proceedings*, 506–509.

Okamoto, K., and S. Shige, 2008: TRMM Precipitation Radar and its observation results. *IEICE Trans. Commun*., **J91-B**, 723–733, (in Japanese)

Olson, W. S., Y. Hong, C. D. Kummerow, and J. Turk, 2001: A texturepolarization method for estimating convective-stratiform precipitation area coverage from passive microwave radiometer data. *J. Appl. Meteor.*, **40**, 1577–1591.

Olson, W. S., C. D. Kummerow, S. Yang, G. W. Petty, W.-K. Tao, T. L. Bell, S. A. Braun, Y. Wang, S. E. Lang, D. E. Johnson, and C. Chiu, 2006: Precipitation and latent heating distributions from satellite passive microwave radiometry. Part I: Method and uncertainty estimates. *J. Appl. Meteor.*, **40,** 702–720.

Schumacher, C., and R. A. Houze Jr., 2003: The TRMM Precipitation Radar's view of shallow, isolated rain. *J. Appl. Meteor.*, **42**, 1519–1524.

Short, D. A., and G. R. North, 1990: The beam filling error in the Nimbus 5 Electronically Scanning Microwave Radiometer observations of Global Atlantic Tropical Experiment rainfall, *J. Geophys. Res*., **95,** 2187–2194.

Short, D. A., and K. Nakamura, 2000: TRMM radar observations of shallow precipitation over the tropical oceans. *J. Climate*, **13**, 4107–4124.

Spencer, R. W., H. M. Goodman, and R. E. Hood, 1989: Precipitation retrieval over land and ocean with SSM/I: Identification and characteristics of the scattering signal. *J. Atmos. Oceanic Technol*., **6**, 2, 254–273.

Steiner, M., R. A. Houze Jr., and S. E. Yuter, 1995: Climatological characterization of three-dimensional storm structure from operational radar

and rain gauge data. *J. Appl. Meteor.*, **34**, 1978–2007.

Turk, J., F. S. Marzano, and A. Mugnai, 1998: Effects of degraded sensor resolution upon passive microwave precipitation retrievals of tropical rainfall, *J. Atmos. Sci*., **55**, 9, 1689–1706.

Varma, A. K., G. Liu, and Y.-J. Noh, 2004: Subpixel-scale variability of rainfall and its application to mitigate the beam-filling problem, *J. Geophys. Res*., **109**, D18210, doi:10.1029/2004JD004968.

Varma, A. K., and G. Liu, 2006: Small-scale horizontal rain-rate variability observed by satellite, *Mon. Wea. Rev*., **134**, 2722–2733.

Wilheit, T. T., 1986: Some comments on passive microwave measurement of rain, *Bull. Amer. Meteor. Soc*., **67**, 1226–1232.